A five-membered $PdSb_n$ coordination series

Andrew Jolleys,[†] Benjamin R. M. Lake,[†] Tobias Krämer[‡]* and Sophie L. Benjamin[†]*

[†]*Department of Chemistry and Forensics, Nottingham Trent University, Clifton Lane, Nottingham NG11 8NS, United Kingdom;* [‡]*Department of Chemistry, Maynooth University, Maynooth, Co Kildare, Ireland*

Keywords

Coordination series · Crystal structure · Secondary bonding · Electronic structure

Abstract

Five complexes of the general formula $PdCl_2(SbMe_2Cl)_n$ (n = 1-5) have been synthesised by combining $[PdCl_2(MeCN)_2]$ and $SbMe_2Cl$ in different molar ratios in toluene. Their solid-state structures have been determined by X-ray crystallography. The complexes display considerable structural diversity: $[Pd_4Cl_8(SbMe_2Cl)_4]$ (**1**, n = 1) is a chloride bridged tetramer, $[Pd_2Cl_4(SbMe_2Cl)_4]$ (**2**, n = 2) is a dimer, $[PdCl(SbMe_2Cl)_2(SbMe_2Cl_2)]$ (**3**, n = 3) is a supramolecular polymer, $[Pd_2(SbMe_2Cl)_8]Cl_4$ (**4**, n = 4) is a loosely associated dimer and $[Pd(SbMe_2Cl)_5]Cl_2$ (**5**, n = 5) is a monomer with square pyramidal $PdSb_5$ coordination geometry. Each structure contains secondary interactions between coordinated Sb centres and chloride ligands or anions, resulting in five-coordinate Sb in all cases with a range of Sb···Cl bond lengths. The electronic structures of these complexes have been investigated using DFT methods including NBO and Pipek-Mezey localised orbital methods in order to interrogate both the Sb-Pd and secondary Sb···Cl bonding.

Introduction

Molecules containing a Lewis acidic main group metal (E) in close proximity to a transition metal (M) have received significant recent attention, particularly examples in which M–E interactions can be used to mediate the electronic properties of M. This can lead to stabilisation of unusual structures and manifestation of new or enhanced cooperative catalytic properties.[1-5] In the majority of cases these are best characterised as M→E interactions, in which M donates electron density to a strongly Lewis acidic E centre. We have an interest in Lewis amphoteric main group ligands, which behave as electron donors towards M, (E→M) while also retaining some Lewis acidic character at E. This behavior is most often observed in complexes of organoantimony ligands, in which Sb(III) centres coordinate to a transition metal via a lone pair while also forming secondary coordinative bonds with available nearby donor atoms (N, O, halides) (Figure 1a).[6-9]

Sb–M (M = late transition metal) complexes can demonstrate unforeseen reactivity arising from the non-innocence of antimony ligands with respect to redox or coordination, as demonstrated by Gabbaï's extensive work on tethered Sb–M systems, leading to potential applications in catalysis, solar energy storage and anion sensing.[3, 10-16] In particular, the strong affinity of Sb for halide anions (X^-) means that the formation of Sb–X bonds is often favoured over the formation of M–X bonds.

The introduction of covalently bonded halide substituents at Sb increases the Lewis acidity of the antimony centre, making halostibines SbR_2X attractive ligands for investigation of Lewis amphoteric behavior. We have previously reported one of the first examples of a halostibine complex with a transition metal halide, $[Pd_2Cl_4(SbMe_2Cl)_4]$ (**2**, Figure 1b), a dimer in the solid-state with two eclipsing square planes held together by secondary Cl→Sb interactions.[17] Reaction of this complex with MeLi

results in the formation of the Pd(0) tetramer $[Pd_4(SbMe_3)_8]$, an unprecedented example of μ_3-bridging by a pnictine ligand (Figure 1b).

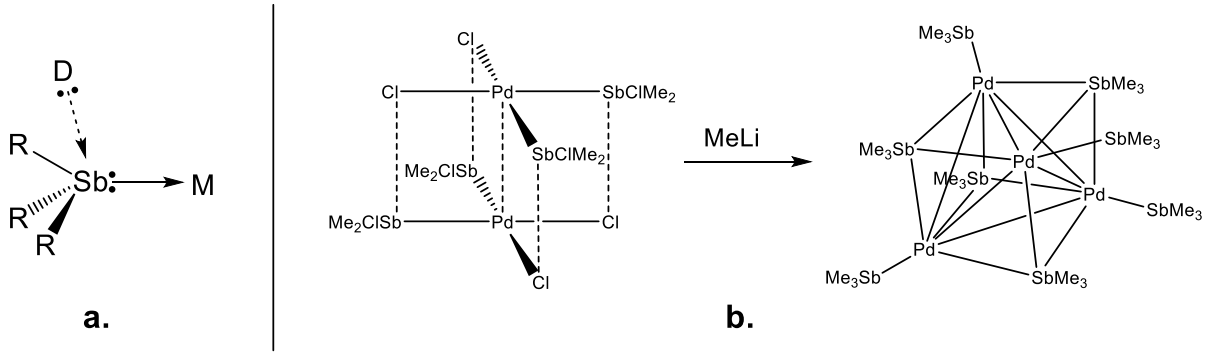

Figure 1 a. Lewis amphoteric behavior of a stibine ligand (D = donor atom, M = transition metal). **b.** Reaction of the dimeric $[Pd_2Cl_4(SbMe_2Cl)_4]$ (**2**, secondary bonding indicated by dashed lines) to form the $[Pd_4(SbMe_3)_8]$ cluster.[17]

Here we report an unusual coordination series of five complexes with the general formula $PdCl_2(SbMe_2Cl)_n$ (n = 1-5), of which **2** is one member (n=2), formed by reacting the same ligand and metal precursor in five different molar ratios. All show Lewis amphoterism of the Sb centres, with either intra- or intermolecular secondary interactions which direct their solid-state structures, leading in four cases to supramolecular architectures. These complexes encompass five different coordination environments of Pd: four square planar with $PdSb_nCl_{(4-n)}$ coordination, and most remarkably the square pyramidal Pd(II) complex **5** which displays homoleptic $PdSb_5$ coordination. This series represents a significant increase in known transition metal complexes with halostibines, and provides an opportunity to investigate and characterise both Sb-M bonding and secondary Cl→Sb bonding in this type of complex.

Results and Discussion

By combining $SbMe_2Cl$ (L) with $[PdCl_2(MeCN)_2]$ (M) in toluene in a range of L:M ratios, five different complexes (**1**-**5**, Scheme 1) were isolated with Sb:Pd ratios of 1:1, 2:1, 3:1, 4:1 and 5:1, and their solid-state structures determined by X-ray crystallography. The structure of each complex is stabilised by secondary Cl→Sb interactions formed by coordinated Sb centres accepting electron density from chloride ligands or anions. The bonding situation in these complexes has been elucidated by DFT analysis of their electronic structure.

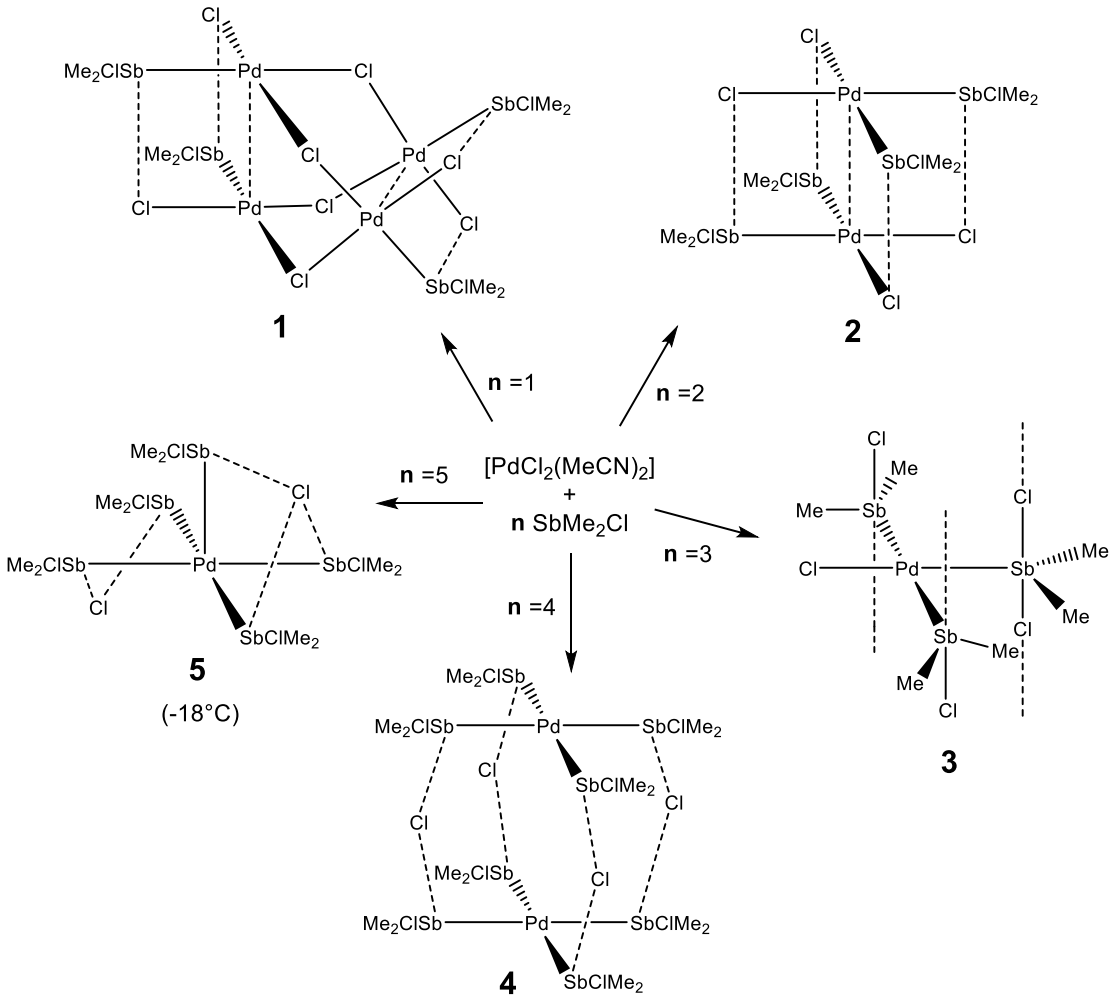

Scheme 1. Synthesis of complexes **1-5** including diagrammatic representation of their solid-state structures.

Combining one equivalent of ligand with the metal precursor resulted in the formation of a near-insoluble red-brown solid, identified by X-ray diffraction as $[Pd_4Cl_8(SbMe_2Cl)_4]$ (**1**), a tetrameric complex with a 1:1 Sb:Pd ratio. The solid-state structure of **1** (Figure 2) contains two pairs of Pd atoms, each pair held together by a combination of one metallophilic Pd···Pd contact (mean Pd-Pd 3.062 Å) and two secondary Cl→Sb interactions between the Cl and $SbMe_2Cl$ ligands on each Pd (mean Sb-Cl 2.947 Å). The two pairs are linked by a total of four Pd–Cl–Pd bridges (mean Pd–Cl 2.365 Å) forming a distorted gyrobifastigium[18] Pd_4Cl_4 core. Despite the pseudo-S_4 symmetry of the molecule (Figure 2, inset), each of the four $PdCl_2(SbMe_2Cl)$ units is crystallographically independent. Comparison of the bond lengths and angles show them to be essentially chemically identical, with the largest variation being a spread of 0.17 Å in the Sb···ClPd distances (Table S7).

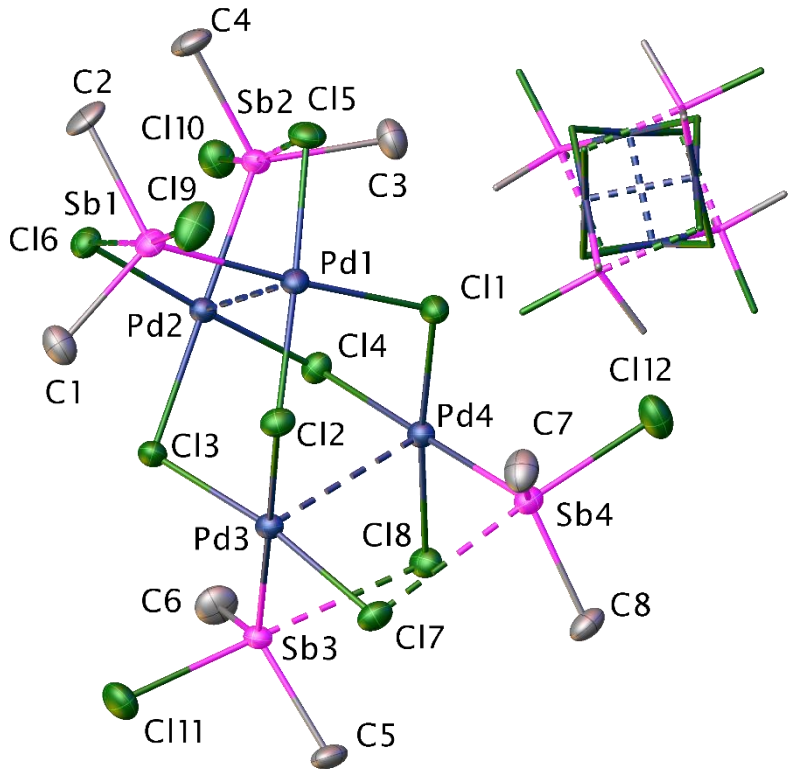

Figure 2 View of the structure of $[Pd_4Cl_8(SbMe_2Cl)_4]$ (**1**), ellipsoids are drawn at 50% probability levels and H atoms are omitted for clarity. Secondary interactions are indicated by dashed bonds. **Inset:** wireframe representation of the view down the pseudo-S_4 axis.

As previously reported,[17] combination of the same two reagents in a 2:1 Sb:Pd ratio gives the red dimer $[Pd_2Cl_4(SbMe_2Cl)_4]$ (**2**). Recrystallisation of this complex from benzene or dichloromethane results in the formation of the respective solvates, **2**·$4C_6H_6$ and **2**·$2CH_2Cl_2$ (Figure 3) whose solid-state structures both contain centrosymmetric dimeric units similar to that found in the unsolvated complex. Though most bond lengths in the three structures are comparable (Tables S8-S11), there is a notable difference in the bond angles around the Sb centres, with Cl–SbSb–Cl torsion angles ranging from 27.74(3)° in the unsolvated structure to 2.65(3)° in the CH_2Cl_2 solvate, the benzene solvate having an intermediate value of 9.21(6)° (Figure 4). There is no evidence of any significant interaction between the dimers and the solvent molecules, so these small differences in structure are most likely to be due to packing effects. The dimers are supported by both Pd···Pd and Cl→Sb interactions, the resulting four membered (–Pd–Sb···Cl–Pd–) ring motif being comparable with that found in complex **1**, with a slightly shorter average Pd···Pd distance (2.918 Å across all three structures, compared to 3.062 Å). In one case, a few yellow crystals were isolated from the second filtrate of this reaction, which were analysed by X-ray crystallography and proved to be the 4:1 L:M complex $[Pd_2(SbMe_2Cl)_8]Cl_4$ (**4**, *vide infra)*.

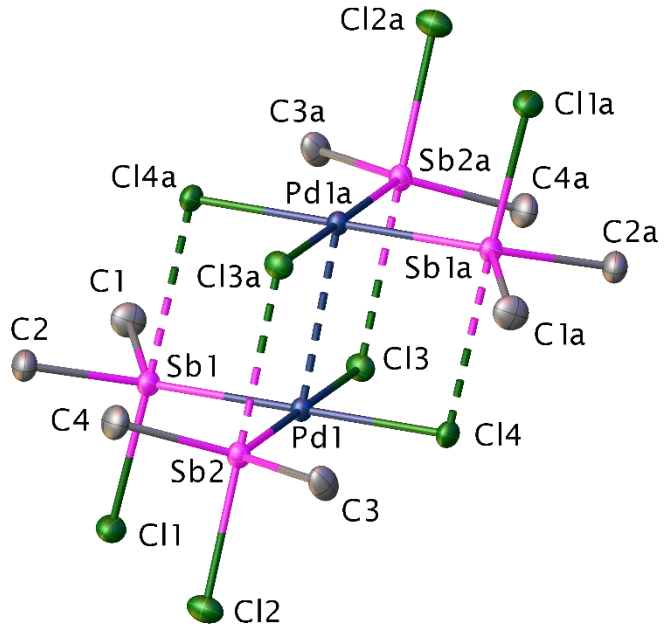

Figure 3 View of the $[Pd_2Cl_4(SbMe_2Cl)_4]$ component of the structure of **2**·$2CH_2Cl_2$, ellipsoids are drawn at 50% probability levels and H atoms are omitted for clarity. Secondary interactions are indicated by dashed bonds. Symmetry operation a = 1-x, 1-y, -z.

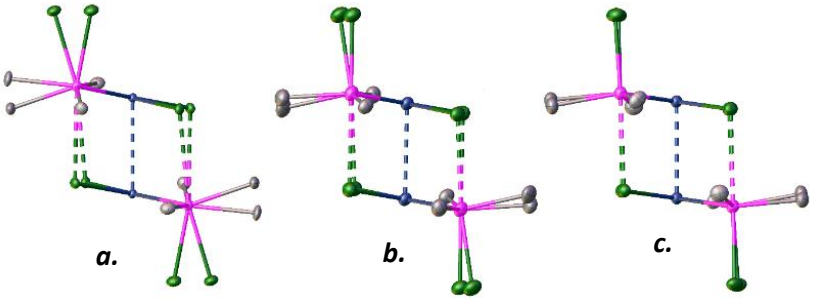

Figure 4 View down the Sb-Sb vector of **2** with the Pd···Pd axis lying vertical in the plane of the page in ***a.*** **2**; ***b.*** **2**·$4C_6H_6$; ***c.*** **2**·$2CH_2Cl_2$.

Increasing the ratio of $SbMe_2Cl$ and $[PdCl_2(MeCN)_2]$ to 3:1 in the reaction mixture results in the isolation of an orange-yellow crystalline solid **3**. The asymmetric unit of the solid-state structure has the formula $[PdCl(SbMe_2Cl)_2(SbMe_2Cl_2)]$, with a 1:3 ratio of Pd:Sb (Figure 5a). The distorted square-planar Pd centre is coordinated by one chloride and two $SbMe_2Cl$ ligands, as well as a moiety which can be tentatively considered as the $SbMe_2Cl_2^-$ ligand, the result of insertion of a third equivalent of $SbMe_2Cl$ into a Pd–Cl bond. The geometry around Sb in this ligand is close to trigonal bipyramidal, with the two Cl substituents *trans* (Cl–Sb–Cl = 176.70(5)°) and the two Sb–Cl distances near equal (2.538(1) Å and 2.590(1) Å) and longer than those in the $SbMe_2Cl$ co-ligands by around 0.2 Å. The two Me substituents lie in an equatorial plane with the Pd centre, with the C–Sb–C angle (106.3(2)°) notably smaller than the C–Sb–Pd angles (mean 126.8°). The only previous complex of this ligand to be structurally characterised is $[FeCp(CO)(PMe_3)(SbMe_2Cl_2)]$,[19] obtained by oxidation of the $SbMe_2^-$ ligand in situ, which has a similar geometry around Sb and a slightly longer mean Sb–Cl distance of 2.601 Å.

Individual molecules of **3** are linked together by Cl→Sb interactions between the Sb atoms of the $SbMe_2Cl$ ligands and the Cl atoms of the $Sb_2MeCl_2^-$ ligands, resulting in a 1D polymeric chain

structure (Sb3–Cl3 = 3.167 Å, Sb1–Cl4 = 3.046 Å). Each molecule forms a total of four intermolecular interactions, two above and two below the square plane, to give a ladder configuration (Figure 5b). In contrast to the structures above, no palladophilic interactions are observed, with the Pd centres in neighbouring molecules being offset from each other with respect to the axis of chain formation (Pd–Pd distances = 6.188, 6.409 Å).

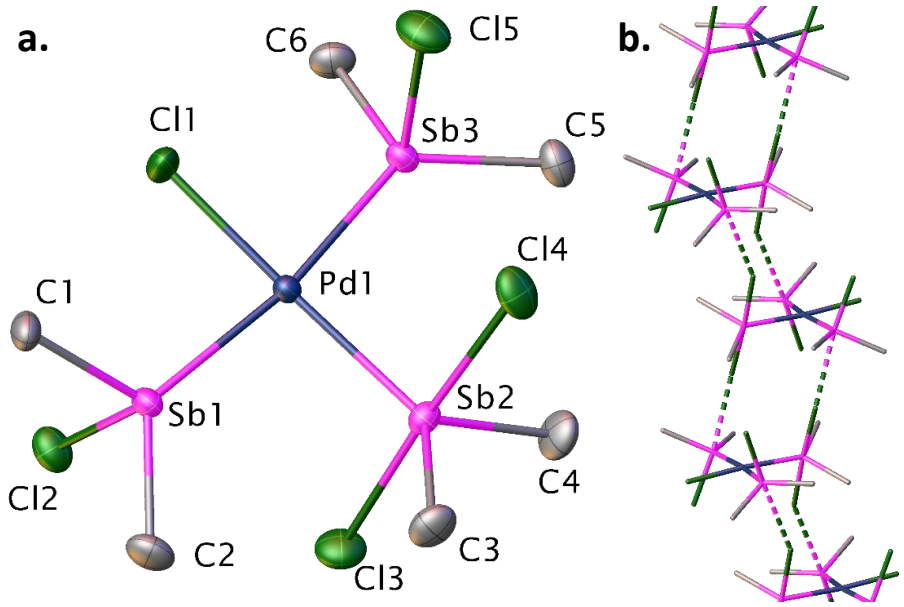

Figure 5 a. View of the asymmetric unit of **3**, ellipsoids are drawn at 50% probability levels and H atoms are omitted for clarity. **b.** Wireframe representation of a section of the 1D ladder structure of **3**. Secondary interactions are indicated by dashed bonds.

It is notable that despite the solid-state structure containing two different Me environments, this complex dissolves in dichloromethane to give an orange solution with only one peak observed in both the ^{1}H and ^{13}C NMR spectra, suggesting that this structure is not retained in solution, or that ligand exchange is fast for both the $SbMe_2Cl$ and $SbMe_2Cl_2^-$ ligands. It is also possible that the two ligand types are interchangeable in solution, with Cl being exchanged between Sb centres on the NMR timescale. Complex **3** seems stable as a solid in air over a period of days, retaining its appearance and structure (according to X-ray powder diffraction).

A detailed analysis of the electronic structure of compound **3** has been undertaken in order to elucidate the nature of the Pd-L bonding. The geometries of **3** and other complexes discussed in this section were optimised (RI-BP86-D3/def2-TZVP(ecp)) prior to analysis of their electronic structures by means of the Natural Bond Orbital (NBO) and Pipek-Mezey localised orbital methods. All calculations were performed *in vacuo* on the isolated molecules. Optimised key bond metrics (Pd–Sb = 2.54-2.56 Å; Pd–Cl1 = 2.35 Å) are in excellent agreement with their crystallographic counterparts (Table S5), also well reproducing the trigonal-bipyramidal geometry around Sb2 (Sb2–Cl3/Cl4 = 2.54 Å; Cl3–Sb2–Cl4 = 177.2°, C3–Sb2–C4 = 108.6°). While the Sb(III) oxidation state and dative character of the $SbMe_2Cl$ ligands seems unambiguous, the situation is less clear-cut for the $SbMe_2Cl_2$ moiety, where the bonding interaction may lie on a continuum between covalent and dative depending on the Sb oxidation state. The recently reported [(*o*-dppp)$_2$Cl$_2$SbPdCl][20] (*o*-dppp = *o*-(Ph_2P)C_6H_4) contains an analogous R_2Cl_2SbPd motif within a polydentate ligand framework, and the Pd–Sb interaction has been characterised as a non-polar covalent bond between formal Sb(IV) and Pd(I) centres, based on analysis of the Natural Localised Bond Orbitals (NLMO) of the Pt homologue.[11]

In the present study an alternative molecular orbital localisation scheme based on the Pipek-Mezey (PM) criterion was utilised in addition to the NBO analysis. The former procedure not only provides the shape of the orbital but also its centroid of charge, which can be used to establish the electron counts of the bonding atoms. For covalent two-centre bonds the orbital charge centroid sits approximately at the centre of the bond vector, while in dative interactions the charge centre is moved closer towards the donor atom.[21, 22]

The [(*o*-dppp)$_2$Cl$_2$SbPdCl] complex serves as a convenient reference point, and is therefore revisited here. The NLMO of the Pd–Sb interaction in [(*o*-dppp)$_2$Cl$_2$SbPdCl] (Figure 6a) is consistent with a covalent σ–type Sb–Pd bond, with orbital contributions of both atoms (Pd 42.5%; Sb 50.1%) being similar to those of the Pt homologue (Pt 45.0%; Sb 49.0%). In both cases the σ-bond is slightly polarised towards antimony.[3] This view finds further support in the corresponding PM localised orbital, with a near tubular shape along the bond vector and a charge centroid positioned nearly equidistantly in between the Pd and Sb atoms (Figure 6a).

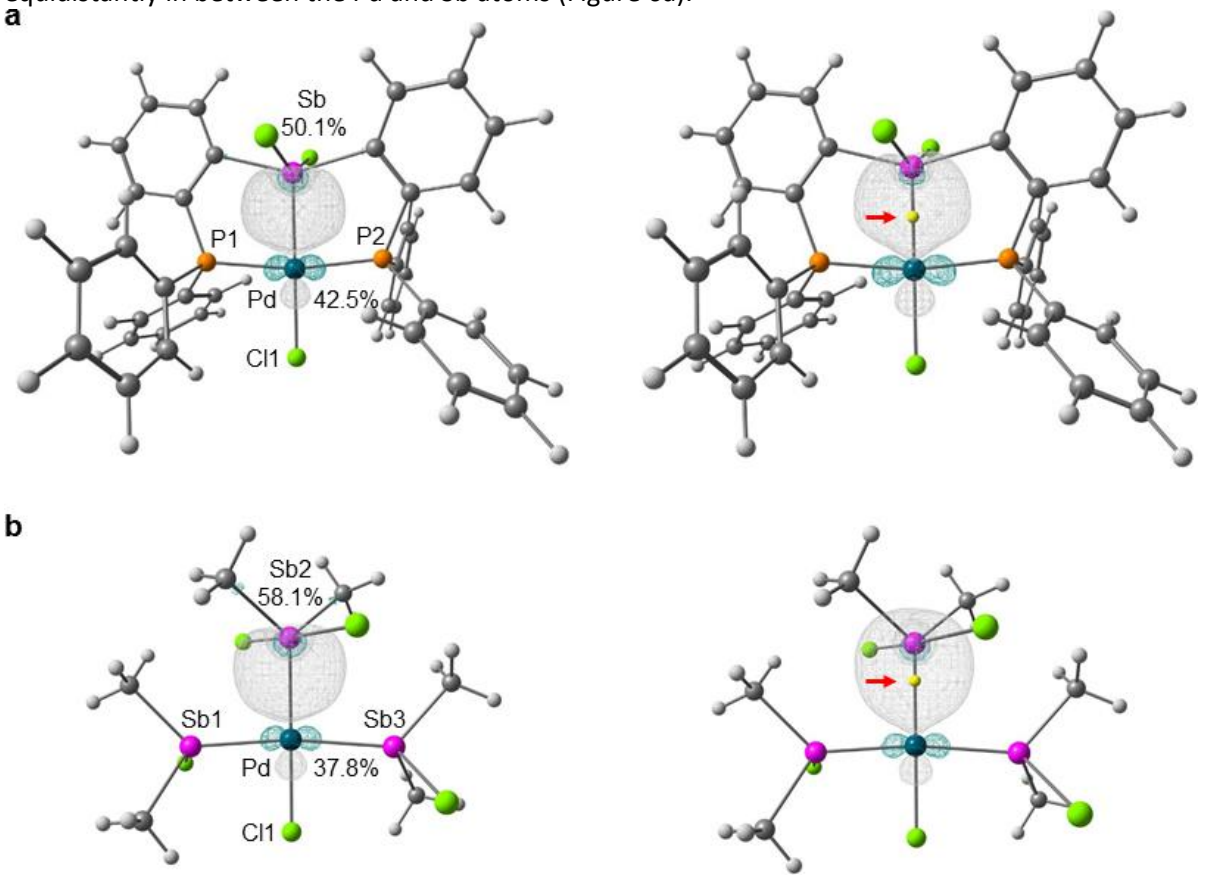

Figure 6 Isosurface plots (cutoff 0.05 a.u.) of NLMOs (left) and Pipek-Mezey localised orbitals (right) for the Pd–Sb interaction in (**a**) [(*o*-dppp)$_2$Cl$_2$SbPdCl] and (**b**) complex **3**. Charge centroids of Pipek-Mezey localised orbitals are shown as yellow dots (red arrows are provided as a guide to the eye). Each dot accounts for two electrons.

In contrast, the PM orbitals and charge centres associated with the Pd–P and Pd–Cl bonds in this complex are notably more displaced towards the P and Cl donors (Figure S2). The dative character of these bonds is also reflected in the associated low Mulliken electron populations on the Pd atom (Table S1), while the electron populations associated with the Pd–Sb bond again display only a slight polarisation towards the Sb centre. The situation differs for complex **3**, in which all PM localised orbitals have more pronounced “pear shapes” weighted towards the donor atoms (Figure S4). The Pd1–Sb2 interaction is very similar to the lone pair dative bonds linking the other donor atoms to Pd,

and the charge centroid is notably shifted towards Sb2 (Figure 6b). The corresponding NLMO converges to the same result, with orbital contributions of both atoms (Pd1 37.8%; Sb3 58.1%) pointing to a dative bond. The resemblance to the bonds involving the $SbMe_2Cl$ ligands is also borne out in the Mulliken populations, which are virtually identical for all three Pd–Sb bonds (Table S2, Pd ~0.45 Sb ~1.65). Thus, the above analysis is in this case fully consistent with a Pd(II) centre ligated by a $Sb^{III}Me_2Cl_2^-$ ligand, and the complex is best described as $[Pd^{II}Cl(Sb^{III}Me_2Cl_2^-)(Sb^{III}Me_2Cl)_2]$. It is interesting to notice that the phenylene bridge in $[(o\text{-dppp})_2Cl_2SbPdCl]$ gives rise to a wider C–Sb–C angle (151.2°), whilst the Cl–Sb–Cl angle becomes more obtuse (151.8°) compared to the corresponding angles in **3** (108.6° and 177.2°). As a result, the approximately trigonal-bipyramidal Sb centre in **3** (τ_5 ~ 0.86) is distorted towards a square-pyramidal geometry (τ_5 ~ 0.0) in $[(o\text{-dppp})_2Cl_2SbPdCl]$. This "$C_{4v}$ distortion" along the described coordinate reduces the proportion of s-character in the σ Pd–Sb bond (28.1%, cf. 39.2% in **3**), which in turn renders the bond less polarised. The presence of a hypervalent $SbMe_2Cl_2^-$ "ate" fragment again appears the best description in $[Fe^{II}Cp(CO)(PMe_3)(SbMe_2Cl_2)]$, which was also modelled for qualitative comparison (Figures S12, S13).

Combination of the precursors in a 4:1 L:M ratio rapidly generates a fine, intensely lemon-yellow precipitate. Isolation of this solid followed by drying in vacuum for 1 hour results in a slight darkening of the colour to orange-yellow. Powder X-ray diffraction of this solid identifies one crystalline phase closely matching the structure of **3** (Figure S11). However, a few small yellow crystals of a dimeric complex with a 4:1 Sb:Pd ratio, $[Pd_2(SbMe_2Cl)_8]Cl_4{\cdot}2C_7H_8$ (**4**, Figure 7), were isolated as a minor product from the (presumably ligand rich) filtrate from the synthesis of **2**. Due to the correspondence in stoichiometry and colour it is presumed that this complex is also a product of the 4:1 reaction, which decomposes under vacuum to generate **3**. Attempts to crystallise **4** in bulk using a variety of solvents and temperatures led only to the isolation of a fine yellow powder, sometimes accompanied by a few crystals of the orange **3** (vide supra) or green **5** (vide infra) complexes. The single crystal X-ray data obtained for **4** is of poor quality and while it allows identification of the structure and connectivity of the complex without doubt, an in-depth analysis of the structural parameters from this data is not appropriate.

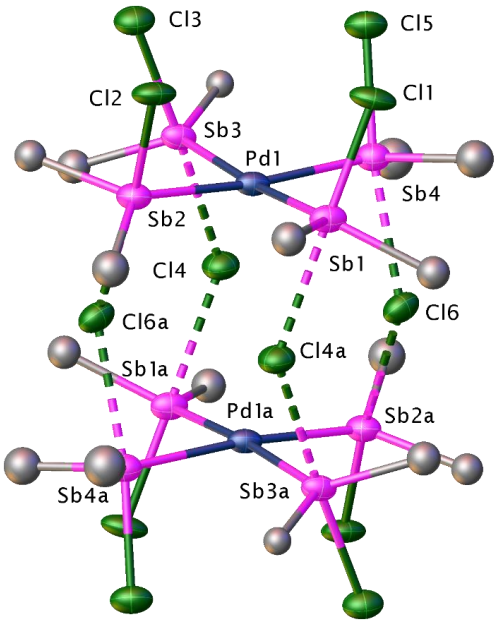

Figure 7 View of **4** from the structure of **4**·$2C_7H_8$. Ellipsoids are drawn at the 50% probability level and H atoms are omitted for clarity. C atoms were refined isotropically. Symmetry operation a = 1-x, 1-y, 1-z. Secondary interactions are indicated by dashed bonds.

The structure is composed of two symmetry-related homoleptic square planar $[Pd(SbMe_2Cl)_4]^{2+}$ cations, with four chloride anions 'sandwiched' between them, each chloride forming two Cl→Sb interactions, one with each cation. The Me substituents of the ligands are found close to the square plane, while the four Cl substituents all face out of the plane on the same side, approximately *trans* to the four longer Cl→Sb interactions on the opposite side. The only other structurally characterised example of a Pd(II) complex with an Sb_4 coordination sphere is in $[Pd\{1,2\text{-}C_6H_4(CH_2SbMe_2)_2\}_2][PF_6]_2$,[23] in which two bidentate distibines chelate the Pd centre. Though the poor quality of our data precludes detailed comparison of the structural parameters, the Sb–Pd bond distances are very similar, averaging around 2.57 Å in both structures. The geometry of **4** has been optimised by DFT methods and the parameters obtained agree well with the X-ray structure (Table S5). The biggest discrepancy is in the long Pd-Pd distance which is calculated to be 0.26 Å shorter than observed in the X-ray data. The Sb···Cl distances are in good agreement, indicating that this is not a result of overestimation of Cl→Sb interaction strength, but rather correlates with a slight underestimate of the Sb-Cl-Sb angles.

Combining greater than four equivalents of $SbMe_2Cl$ with one equivalent of $[PdCl_2(MeCN)_2]$ in toluene at room temperature likewise precipitates a yellow product, which, similarly to the 4:1 reaction, gives crystals of **3** after drying under vacuum, though the elemental analysis of the bulk product suggests higher ligand content. However, refrigeration of the initial filtrate at –18°C causes the solution to become a deep green colour, which on warming back to room temperature reverts to the original yellow. This reversible colour change could be observed repeatedly by cooling and warming the solution. Storage of the solution at -18°C for several days allowed the isolation of a few green-black crystals, which appeared to be stable at room temperature under fomblin oil for several days.

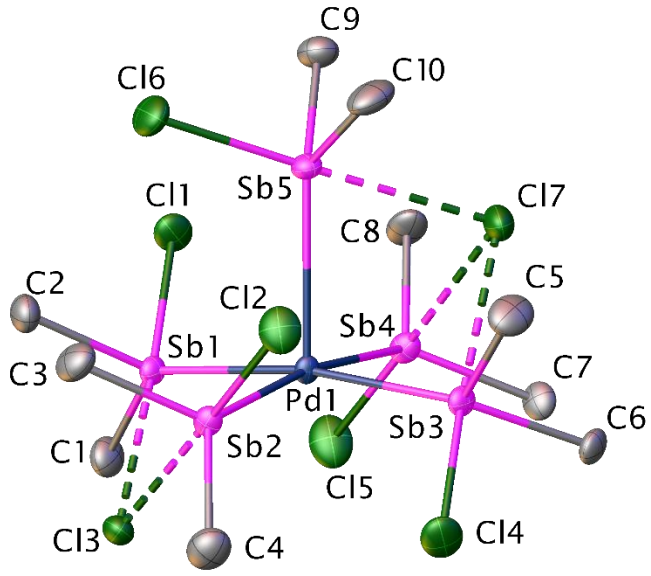

Figure 8 View of the structure of **5**, ellipsoids are drawn at 50% probability levels and H atoms are omitted for clarity. Secondary interactions are indicated by dashed bonds.

The structure was determined by X-ray diffraction and shows the highly unusual monomeric complex $[Pd(SbMe_2Cl)_5]Cl_2$ (**5**, Figure 8), in which five equivalents of the $SbMe_2Cl$ ligand are coordinated to one Pd centre in a distorted square-pyramidal geometry. The Pd atom sits only 0.23 Å above the square plane defined by the four equatorial ligands. The Sb–Pd bond length for the axial ligand (Sb5–Pd1 = 2.971(1) Å) is significantly greater than for the equatorial ligands (2.593-2.599 Å),

and somewhat greater than the sum of the covalent radii (Σr_{cov} =2.78 Å),[24] though much shorter than the sum of the Van der Waals radii (Σr_{VdW} = 4.62 Å).[25] This weaker coordinate bond undoubtedly reflects the energy penalty of disrupting the favoured square planar ligand field for the d^8 metal centre by introducing axial coordination. The two chloride anions form close contacts with the Sb centres of the ligands, this time in an intramolecular fashion, with one chloride bridging two *cis* equatorial ligands below the square plane, and the other bridging the remaining three ligands (two equatorial and one axial) above the plane. Each ligand is arranged so that the covalent Sb–Cl substituent is roughly *trans* to the coordinated chloride anion. This gives the molecule a pseudo mirror plane perpendicular to the equatorial square plane ([Sb1,Sb2,Sb3,Sb4]∠[Pd1,Sb5,Cl6,Cl7,Cl3] = 90.0°), which bisects the two chloride anions, the axially coordinated ligand and the angles between two *cis* pairs of equatorial ligands, though attempts to model the structure in a higher symmetry space group were unsuccessful. Literature precedent for square pyramidal Pd(II) complexes is mostly confined to examples in which the architecture of a polydentate ligand sterically constrains the coordination geometry,[26-28] or where a halide occupies the apical position with a long bond distance.[29, 30] To our knowledge there are no other examples of homoleptic square pyramidal Pd(II) with monodentate ligands. Presumably upon warming to room temperature in solution the weakly associated axial fifth ligand becomes dissociated, returning the complex to a 4-coordinate, square planar configuration and triggering the reversible change in colour.

The nature of the Pd–Sb interactions in complex **5** has been probed using the same methods outlined above for complex **3**. The distorted square-pyramidal geometry is well reproduced in the DFT-optimised structure, with the Pd atom displaced by 0.27 Å above the centre of the equatorial ligand plane. Optimised bond distances are in good agreement with experiment. The asymmetry between the basal Pd–Sb (2.61-2.62 Å) and apical Pd–Sb bond lengths (2.80 Å) is reproduced by the calculations, although the latter is somewhat underestimated compared to the single crystal X-ray data (2.971(2) Å). The bond distances between the chloride anions and the Sb centres of the ligands (Sb···Cl = 2.77-3.17 Å) are also in reasonably good agreement with the experimental values (2.772(4)-3.027(4) Å).

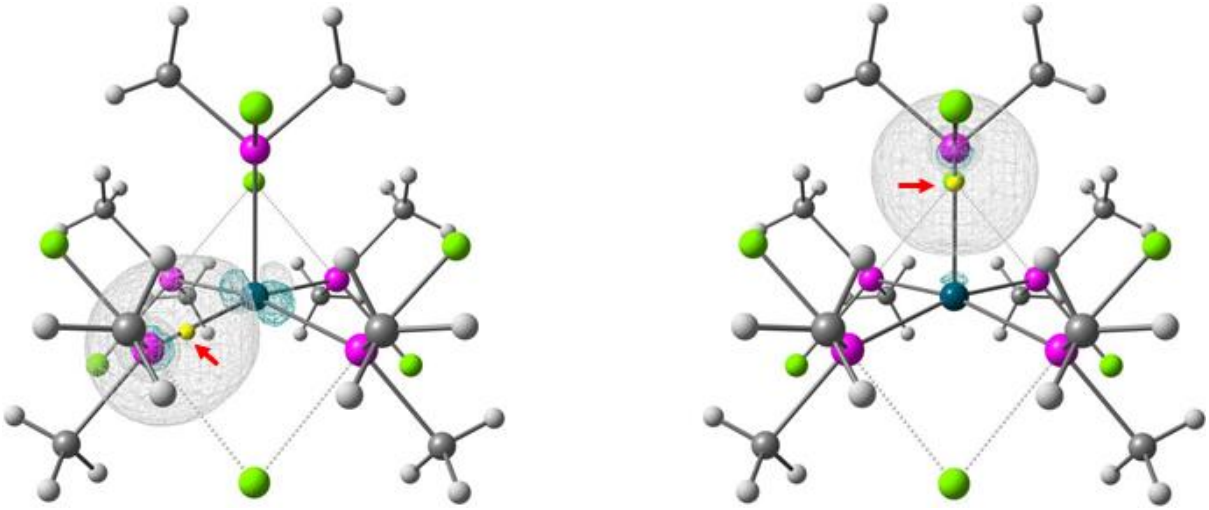

Figure 9 Isosurface plots (cutoff 0.05 a.u.) of Pipek-Mezey localised orbitals for the basal (left) and apical (right) Pd–Sb interactions in complex **5**. Charge centroids of are shown as yellow dots (red arrows are provided as a guide to the eye). Each dot accounts for two electrons.

Both NBO analysis and PM localisation predict the presence of lone-pair dative bonds linking the basal Sb centres to the Pd atom (Figure 9 and Figure S5), comparable to those observed in **3**. On the other hand, the apical Pd–Sb bond may be best described as $lp_{Sb5} \rightarrow Pd\ \sigma^*_{Pd\text{-}Sb}$ donor-acceptor interactions

($\Sigma\Delta E^{(2)}$ = 57.1 kcal mol^{-1}), involving anti-bonding Pd *sd* hybrid orbitals. The lone pair located on the Sb centre obtained from the PM localisation procedure is shown in Figure 9. Importantly, there is no indication of any Pd→p_{Sb} interaction that would support the presence of a Lewis acidic Z-type stiborane ligand. The above analysis is consistent with the experimental result, and clearly distinguishes between two different bond types in the complex, with a weaker bound apical ligand.

Secondary intramolecular donor-acceptor interactions between the Cl^- anions and the coordinated $SbMe_2Cl$ ligands were also readily identified by NBO analysis (see Figure S7 for isosurface plots of key donor-acceptor orbital pairs). The bridging chloride Cl3 is largely stabilised through donation of electron density from one of its 3p donor orbitals into the *trans* $\sigma^*_{Sb\text{-}C}$ orbitals on the two adjacent $SbMe_2Cl$ units ($\Delta E^{(2)}$ = 20.7 kcal mol^{-1} and 22.3 kcal mol^{-1} for Sb1 and Sb2, respectively). Likewise, two such $3p_{Cl}$→$\sigma^*_{Sb\text{-}Cl}$ interactions are observed for Cl7 interacting with the two equatorial stibine fragments. The larger distance between Cl7 and these Sb acceptors (~2.92 Å) compared to Cl3 (~2.77 Å) is reflected in a smaller interaction energy ($\Delta E^{(2)}$ = 13.4 kcal mol^{-1} and 12.9 kcal mol^{-1} for Sb3 and Sb4, respectively). However, a third interaction between an orthogonal $3p_{Cl}$ donor orbital and the $\sigma^*_{Sb\text{-}Cl}$ acceptor orbital located on the axial $SbMe_2Cl$ unit ($\Delta E^{(2)}$ = 11.0 kcal mol^{-1}) adds to the overall stabilization energy ($\Sigma\Delta E^{(2)}$ = 37.3 kcal mol^{-1}) , rendering it similar in magnitude to the sum of the interactions between Cl3 and Sb1/Sb2 ($\Sigma\Delta E^{(2)}$ = 43.0 kcal mol^{-1}). Secondary interactions similar to those found in **5** are also the main contributing factor in supporting the structures of **1** and **2** (Figures S8 and S10). The approximate trans orientation of Pd-bound Cl^- and the Sb–Cl bond of the $SbMe_2Cl$ group on adjacent complex fragments maximizes the $3p_{Cl}$→$\sigma^*_{Sb\text{-}Cl}$ orbital interactions ($\Delta E^{(2)}$ ~ 20 kcal mol^{-1} / pair), which we have previously demonstrated for the 2:1 L:M complex **2** in this series.[16] Additional stabilisation in both the tetrameric and dimeric complexes is provided by cis $3p_{Cl}$→$\sigma^*_{Sb\text{-}C}$ ($\Delta E^{(2)}$ = 2–4 kcal mol^{-1} / pair), and $4d_{Pd}$ →$\sigma^*_{Pd\text{-}L}$ interactions ($\Delta E^{(2)}$ = 0.1–2.5 kcal mol^{-1} / pair). The latter involve mutual donation of electron density from Pd lone pairs (*d*-orbitals) into antibonding Pd–ligand σ* orbitals centred on neighbouring Pd centres. Detailed analysis of canonical and localised molecular orbitals for **1** and **2**, however, does not support the presence of any significant direct Pd-Pd bonding interaction in these complexes (Figures S9 and S11, Table S4).

Secondary bonding at Sb

In all five complexes each $SbMe_2Cl$ ligand forms one secondary Cl→Sb interaction, in every case disposed approximately *trans* to the covalent Sb–Cl bond (mean Cl–Sb···Cl = 174.4°). This is consistent with the acceptor behavior of the $SbMe_2Cl$ ligand observed in other complexes towards heteroatoms (O, F) from 'weakly coordinating' anions, which also coordinate *trans* to the Sb–Cl bond.[6] The complex [CpFe(CO)(Me_2BrSb-μ-Br-$SbBrMe_2$)] also displays very similar interactions between a bromide anion and the related bromostibine ligand, particularly reminiscent of the (–Pd1–Sb1–Cl3–Sb2–) ring found in **5**.[7] As discussed above, this behavior is attributable to the availability of the low lying σ* Sb–X orbital on the halostibine ligand, which acts as an acceptor orbital. The structurally characterised series of complexes described here presents a unique opportunity to compare several examples of secondary interactions between the same ligand with the same metal halide, all in similar coordination environments. Interatomic distances for the secondary Cl→Sb interactions in these complexes range between 2.75-3.17 Å (Σr_{VdW} = 4.29 Å, Σr_{cov} = 2.78 Å).[25, 24] Plotting these distances for all 7 structures against the *trans* covalent Sb–Cl distance for each Sb atom reveals a clear linear trend with a negative gradient (Figure 10), consistent with the increased population of the $\sigma^*_{Sb\text{–}Cl}$ orbital as a result of a stronger Cl→Sb interaction, weakening the *trans* covalent Sb–Cl bond. This corroborates a significant involvement of orbital interactions in forming these secondary, 'hypervalent' bonds, rather than their being entirely the result of electrostatic interactions.

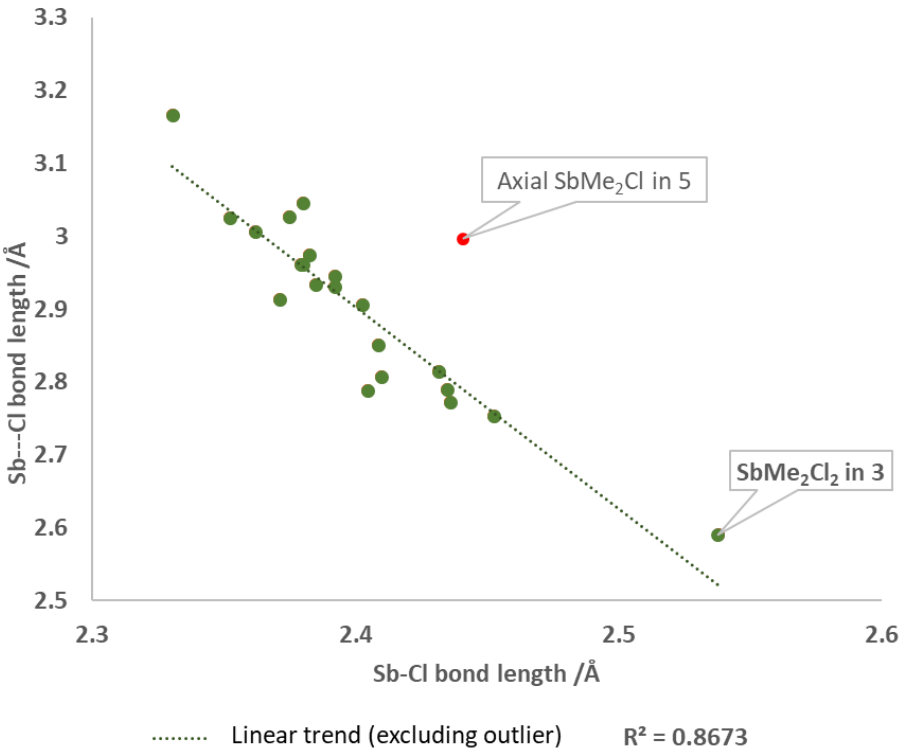

Figure 10 Graph showing secondary Sb···Cl bond distances *vs* the *trans* covalent Sb-Cl distances for all Sb atoms in compounds **1**-**5**.

There is one main outlier which was excluded from the fit, namely the Sb centre which is weakly coordinated to Pd in the axial position in the structure of **5**. This discrepancy can be explained by the significantly different coordination environment of this Sb centre with respect to Pd when compared to the other $SbMe_2Cl$ ligands. Notably, plotting the two near equal Sb–Cl distances around the $SbMe_2Cl_2$ ligand in **3** gives a point which lies in good agreement with the general linear trend, suggesting that this ligand can alternatively be viewed as the result of a strong interaction between a Cl^- anion and a $SbMe_2Cl$ ligand, analogous to the weaker interactions of the same nature seen in **4** and **5**, but to the extent that a near symmetrical 3-centre-4-electron bond is formed.

Solution behavior

In toluene solution, each complex retains the characteristic colour of the corresponding solid, though there is a slight change of colour when complexes **1-3** are dissolved in dichloromethane. The ^{1}H and ^{13}C NMR spectra of **1-3** are almost indistinguishable, each containing a single peak at around 2.1-2.2 ppm (^{1}H NMR) and 16-18 ppm (^{13}C NMR), consistent with a single ligand environment. It is probable that the complexes are fluxional in solution, with the labile $SbMe_2Cl$ ligands exchanging fast on the NMR timescale and the prevalent structure (and hence colour) depending on the L:M ratio in solution. UV-Vis electronic spectra (Figures S16 and S17, Table S17) in dichloromethane solution differ significantly between the three compounds, each displaying two main bands, with those of **1** lying the lowest in energy followed by **2** then **3**. The solid-state spectra are somewhat different, each containing several broad overlapping bands in the 300-600 nm region. To investigate the interconversion of the five compounds in solution, five equivalents of the ligand in a toluene stock solution were sequentially added to the metal precursor, interspersed by 30-40 minute periods of stirring between each equivalent. The colour of the solution changed through red-brown after one equivalent to red after the second, orange after the third and yellow after the fourth, suggesting

these complexes interconvert with facility in solution. Adding a fifth equivalent results in a slight colour change to a less warm yellow, which on refrigeration at –18°C becomes the characteristic intense green of complex **5** (Figure S18).

Conclusions

Complexes **1**-**5** represent a rare example of a coordination series in which the same metal fragment ($PdCl_2$) complexes the same ligand ($SbMe_2Cl$) in five different stoichiometries, without the presence of other coligands. While complexes **1**-**3** are fairly robust, even air stable in the case of **3**, complexes **4** and **5** are unstable with respect to loss of ligand. The bonding in these complexes has been investigated by a combination of crystallographic and computational techniques. Sb–Pd bonding has been characterised as dative, with the largest component of electron density remaining localised at Sb. The Lewis amphoterism of the chlorostibine ligands gives rise to secondary Sb···Cl bonds, observed in the solid-state of all complexes, arising from $lp_{Cl} \rightarrow Sb\ \sigma^*_{Sb\text{-}Cl}$ interactions. In compounds **1**-**4** this secondary bonding drives the formation of supramolecular structures, including two dimers, a tetramer and a polymer. The square pyramidal Pd(II) complex **5** is an unprecedented example of $PdSb_5$ coordination, in which the fifth, axial ligand coordinates via a $lp_{Sb} \rightarrow Pd\ \sigma^*_{Pd\text{-}Sb}$ donor-acceptor interaction.

Experimental

Preparations were undertaken using standard Schlenk and glove box techniques under a N_2 atmosphere. Solvents were dried using a solvent purification system (MBraun SPS 800; toluene, CH_2Cl_2, Et_2O, *n*-hexane) or distillation over sodium wire (benzene) and degassed with N_2 prior to use. $[PdCl_2(MeCN)_2]$ was prepared by refluxing $PdCl_2$ in MeCN, and $SbMe_2Cl$ by a modification of the literature method.[31] ^1H and $^{13}C\{^1H\}$ NMR spectra were recorded using a Jeol Eclipse 400 MHz spectrometer at ambient temperature (25 °C), and are referenced to the residual solvent signal. The purity of the compounds was established by microanalysis on crystalline samples where possible. Microanalyses were performed by London Metropolitan University.

1. $[Pd_4Cl_8(SbMe_2Cl)_4]$

To a stirring suspension of $[PdCl_2(MeCN)_2]$ (0.121 g, 0.466 mmol) in toluene (10 cm^3) was added a solution of $SbMe_2Cl$ (0.47 mmol, 1 equiv.) in toluene (3 cm^3), giving a deep-green suspension that rapidly became red-brown. After stirring at room temperature for 4 days, the dark red-brown product was collected by filtration, washed with hexane (10 cm^3) and dried *in vacuo*. Yield: 0.110 g (0.075 mmol, 65%). Large red-black crystals suitable for X-ray diffraction were obtained by dissolving *ca*. 50 mg of this compound in boiling THF (15 cm^3), concentrating the solution *in vacuo* to *ca*. 50% of its original volume and overlayering with hexane (40 cm^3). ^1H NMR (400 MHz, $CDCl_3$, 293 K): δ 2.22 (24H, s, $(H_3C)_2Sb$). Elemental analysis, calculated for $C_8H_{24}Cl_{12}Pd_4Sb_4$ (%): C, 6.59; H, 1.66. Found: C, 7.19; H, 1.49.

2. $[Pd_2Cl_4(SbMe_2Cl)_4]$ and crystals of 4. $[Pd_2(SbMe_2Cl)_8]Cl_4$

A solution of $SbMe_2Cl$ (2.92 mmol, 2 equiv.) in toluene (35 cm^3) was added directly to solid $[PdCl_2(MeCN)_2]$ (0.373 g, 1.440 mmol), giving a yellow suspension that turned bright-red after *ca*. 2 hours. After stirring at room temperature for 2 days, the bright-red product was collected by filtration, washed with Et_2O and dried *in vacuo*. Yield: 0.502 g (0.455 mmol, 63%). ^1H NMR (400 MHz,

CD_2Cl_2, 293 K): δ 2.22 (24H, s, $(H_3C)_2Sb$). ^{13}C NMR (100 MHz, $CDCl_3$, 293 K): δ 16.3 ($(H_3C)_2Sb$) Altering the procedure so that after the first two hours stirring was stopped and the solution allowed to stand for a few days yielded red prisms of **2** with the previously reported structure.[16] Recrystallisation of the product from CH_2Cl_2 at -18 °C gave rod shaped crystals of the solvate **2**·$2CH_2Cl_2$. Recrystallisation of the product from benzene at room temperature gave a few crystals of the solvate **2**·$4C_6H_6$. On one occasion, after collecting the product the remaining toluene/Et_2O filtrate was concentrated *in vacuo* until a yellow solid began to precipitate. Heating the mixture to boiling caused this to redissolve, furnishing an orange solution, which upon cooling to -18 °C became deep-green in colour. After storage for three days at -18 °C a microcrystalline yellow solid formed. X-ray diffraction analysis (poor quality data) revealed this to be **4**.

3. [PdCl(SbMe$_2$Cl)$_2$(SbMe$_2$Cl$_2$)]

A solution of $SbMe_2Cl$ (0.44 mmol, 3 equiv.) in toluene (10 cm^3) was added to a stirring suspension of $[PdCl_2(MeCN)_2]$ (0.038 g, 0.147 mmol) in toluene (10 cm^3), rapidly forming a bright orange-brown solution that began to deposit solid after *ca*. 15 minutes. After stirring at room temperature for 2 days, the mixture was concentrated *in vacuo* to *ca*. 50% of its original volume, then the orange-yellow product was collected by filtration, washed with hexane (30 cm^3) and dried *in vacuo*. Yield: 0.051 g (0.069 mmol, 47%). ^1H NMR (400 MHz, $CDCl_3$, 293 K): δ 2.13 (18H, s, $(H_3C)_2Sb$). ^{13}C NMR (100 MHz, $CDCl_3$, 293 K): δ 16.27 ($(H_3C)_2Sb$). ^1H NMR (400 MHz, CD_2Cl_2, 293 K): δ 2.11 (18H, s, $(H_3C)_2Sb$). ^{13}C NMR (100 MHz, CD_2Cl_2, 293 K): δ 17.16 ($(H_3C)_2Sb$). Elemental analysis, calculated for $C_6H_{18}Cl_5Pd_1Sb_3$ (%): C, 9.75; H, 2.45. Found: C, 9.82; H, 2.44. Large golden-yellow crystals suitable for X-ray diffraction were obtained via slow diffusion of the layered toluene/hexane filtrate at room temperature.

5. [Pd(SbMe$_2$Cl)$_5$]Cl$_2$

A solution of $SbMe_2Cl$ (2.02 mmol, 4.2 equiv.) in toluene (10 cm^3) was added to a stirring suspension of $[PdCl_2(MeCN)_2]$ (0.126 g, 0.4860 mmol) in toluene (10 cm^3), giving a suspension that was briefly deep-green in colour, rapidly turning bright-yellow. After stirring at room temperature, the yellow product was collected by filtration, washed with hexane (30 cm^3) and dried *in vacuo* during which it was observed to darken slightly. Yield: 0.251 g. ^1H NMR (400 MHz, $CDCl_3$, 293 K): δ 2.11 (48H, s, $(H_3C)_2Sb$). ^{13}C NMR (100 MHz, $CDCl_3$, 293 K): δ 16.47 ($(H_3C)_2Sb$). Recrystallisation from this solid gave crystals of **3** only. Elemental analysis, calculated for **3** $C_6H_{18}Cl_5Pd_1Sb_3$ (%): C, 9.75; H, 2.45; for **4** $C_{16}H_{48}Cl_{12}Pd_2Sb_8$: C, 10.37; H, 2.61; for **5** $C_{10}H_{30}Cl_7Pd_1Sb_5$: C, 10.78; H, 2.72. Found: C, 10.52; H, 2.34. Cooling the layered toluene/hexane filtrate to -18 °C caused the toluene layer to rapidly change colour from yellow to deep-green, and after storage at -18 °C for three days a few large, very dark green crystals formed. These were determined by X-ray crystallography to be $[Pd(SbMe_2Cl)_5]Cl_2$. Warming of the solution returned it to a yellow colour. Repeating the experiment with up to 5.5 equivalents of $SbMe_2Cl$ gave very similar results.

Attempted direct preparation of 4. resulting in decomposition to 3.

A solution of $SbMe_2Cl$ (1.82 mmol, 4 equiv.) in toluene (10 cm^3) was added directly to solid $[PdCl_2(MeCN)_2]$ (0.117 g, 0.451 mmol), giving a deep-green suspension that turned bright-yellow within a few minutes. After stirring at room temperature for 1 day, the lemon-yellow product was collected by filtration and washed with Et_2O (10 cm^3). After drying *in vacuo* a slight darkening to orange-yellow was observed. Powder XRD of the dried product matched that predicted for complex **3**, with no other phases identified. Yield: 0.254 g (0.344 mmol, 76 % vs Pd). Elemental analysis, calculated for $C_6H_{18}Cl_5Pd_1Sb_3$ (%): C, 9.75; H, 2.45. Found: C, 9.89; H, 2.22.

Computational Methods

Unconstrained geometry optimisations and subsequent frequency calculations of all complexes were carried out at the DFT level using ORCA 4.0.0.2.[32] These calculations employed the BP86 GGA functional[33, 34] in conjunction with the RI-J approximation.[35-37] The def2-TZVP basis set was used on all atoms,[37] combined with the corresponding Weigend *J* auxiliary basis.[39] Core electrons of heavier elements (Pd[40], Sb[41]) were replaced by the appropriate relativistic def2-ECP effective core potentials. Dispersion effects were accounted for by including Grimme's DFT-D3 method in combination with Becke-Johnson damping (D3BJ).[42, 43] Stationary points were confirmed to be minima by the absence of imaginary frequencies. The electronic structure of the complexes was analysed by means of localized molecular orbitals, generated with the Pipek-Mezey method,[44] and Natural Bond Orbitals (NBO6).[45] These calculations utilised both the ORCA 4.0.0.2 and Gaussian09 (rev D.01) software,[46] employing the same level of theory as described above to calculate the required wave functions on the DFT-optimised geometries.

Crystallographic methods

Data collections were carried out using either an Oxford Xcalibur Gemini diffractometer equipped with a Sapphire3 CCD detector at a temperature of 100K or a Rigaku AFC12 goniometer equipped with an enhanced sensitivity (HG) Saturn724+ detector at a temperature of 150 K. Refinement details and crystallographic parameters can be found in the supplementary information file. The CCDC deposition numbers 1853471-1853475 contain the supplementary crystallographic data for this paper. These data are provided free of charge by the Cambridge Crystallographic Data Centre.

Acknowledgements

This work was partially funded by EPSRC grant EP/R020418/1. We thank Prof. Stuart A. Macgregor (Heriot Watt University) for providing access to high performance computing facilities. We also thank Prof. W. Levason and Prof. G. Reid (University of Southampton) for helpful discussions.

Supporting information

Detailed computational information, crystallographic information, UV-vis spectra, NMR spectra, photographs of reaction solutions.

Author information

Corresponding authors:

*Sophie Benjamin sophie.benjamin@ntu.ac.uk (experimental)

*Tobias Krämer tobias.kraemer@mu.ie (theoretical)

The authors declare no competing financial interests.

References

1. Vollmer, M. V.; Xie, J.; Lu, C. C. *J. Am. Chem. Soc.* **2017**, *139*, 6570-6573.

2. Cammarota, R. C.; Lu, C. C. *J. Am. Chem. Soc.* **2015**, *137*, 12486-12489.

3. You, D.; Gabbaï, F. P. *J. Am. Chem. Soc.* **2017**, *139*, 6843-6846.

4. Jones, J. S.; Gabbaï, F. P. *Chem. Eur. J.* **2017**, *23*, 1136-1144.

5. Devillard, M.; Declercq, R.; Nicolas, E., Ehlers, A. W.; Backs, J.; Saffon-Merceron, N.; Bouhadir, G.; Slootweg, J. C.; Uhl, W.; Bourissou, D. *J. Am. Chem. Soc.* **2016***, 138*, 4917-4926.

6. Benjamin, S. L.; Reid, G. *Coord. Chem. Rev.* **2015***, 297–298*, 168-180.

7. Benjamin, S. L.; Levason, W.; Light, M. E.; Reid, G.; Rogers, S. M. *Organometallics* **2014***, 33*, 2693-2695.

8. Benjamin, S. L.; Levason, W.; Reid, G.; Warr, R. P. *Organometallics* **2012***, 31*, 1025-1034.

9. Benjamin, S. L.; Karagiannidis, L.; Levason, W.; Reid, G.; Rogers, M. C. *Organometallics* **2011***, 30*, 895-904.

10. Wade, C. R.; Ke, I.; Gabbaï, F. P. *Angew. Chem. Int. Edit.* **2012***, 51*, 478-481.

11. Yang, H.; Gabbaï, F. P. *J. Am. Chem. Soc.* **2014***, 136*, 10866-10869.

12. Jones, J. S.; Wade, C. R.; Yang, M.; Gabbaï, F. P. *Dalton Trans.* **2017***, 46*, 5598-5604.

13. Ke, I.; Jones, J. S.; Gabbaï, F. P. *Angew. Chem. Int. Edit.* **2014***, 53*, 2633-2637.

14. Jones, J. S.; Gabbaï, F. P. *Acc. Chem. Res.* **2016***, 49*, 857-867.

15. You, D.; Yang, H.; Sen, S.; Gabbaï, F. P. *J. Am. Chem. Soc.* **2018**, *140*, 9644-9651.

16. Yang, H.; Gabbaï, F. P. *J. Am. Chem. Soc.* **2015**, 137, 41, 1345-1342

17. Benjamin, S. L.; Krämer, T.; Levason, W.; Light, M. E.; Macgregor, S. A.; Reid, G. *J. Am. Chem. Soc.* **2016***, 138*, 6964-6967.

18. Alvarez, S. *Coord. Chem. Rev.* **2017***, 350*, 3-13.

19. Malisch, W.; Kaul, H.; Gross, E.; Thewalt, U. *Angew. Chem. Int. Edit. Engl.* **1982***, 21*, 549-550.

20. Sahu, S.; Gabbaï, F. P. *J. Am. Chem. Soc.* **2017***, 139*, 5035-5038.

21. Vidossich, P.; Lledos, A. *Dalton Trans.* **2014***, 43*, 11145-11151.

22. Sit, P. H.; Car, R.; Cohen, M. H.; Selloni, A. *Inorg. Chem.* **2011***, 50*, 10259-10267.

23. Levason, W.; Matthews, M. L.; Reid, G.; Webster, M. *Dalton Trans.* **2004**, 554-561.

24. Cordero, B.; Gomez, V.; Platero-Prats, A.; Reves, M.; Echeverria, J.; Cremades, E.; Barragan, F.; Alvarez, S. *Dalton Trans.* **2008**, 2832-2838.

25. Alvarez, S. *Dalton Trans.* **2013***, 42*, 8617-8636.

26. Hubin, T. J.; Alcock, N. W.; Busch, D. H. *Acta Cryst. C* **1999***, 55*, 1404-1406.

27. Blake, A. J.; Roberts, Y. V.; Schroder, M. *J. Chem. Soc. Dalton Trans.* **1996**, 1885-1895.

28. Blundell, T. L.; Powell, H. M. *J. Chem. Soc. A* **1967**, 1650-1657.

29. Chui, K. M.; Powell, H. M. *J. Chem. Soc. Dalton Trans.* **1974**, 2117-2122.

30. Sevillano, P.; Habtemariam, A.; Castiñeiras, A.; García, M. E.; Sadler, P. J. *Polyhedron* **1998***, 18*, 383-389.

31. Breunig, H. J.; Althaus, H.; Rosler, R.; Lork, E. *Z. Anorg. Allg. Chem.* **2000***, 626*, 1137-1140.

32. Neese, F. *WIREs Comput. Mol. Sci.* **2018***, 8*, e1327.

33. Becke, A. D. *Phys. Rev. A* **1988***, 38*, 3098-3100.

34. Perdew, J. P. *Phys. Rev. B* **1986***, 33*, 8822-8824.

35. Dunlap, B. I.; Connolly, J. W. D.; Sabin, J. R. *J. Chem. Phys.* **1979***, 71*, 3396-3402.

36. Vahtras, O.; Almlöf, J.; Feyereisen, M. W. *Chem. Phys. Lett.* **1993***, 213*, 514-518.

37. Neese, F. *J. Comput. Chem.* **2003***, 24*, 1740-1747.

38. Weigend, F.; Ahlrichs, R. *Phys. Chem. Chem. Phys.* **2005***, 7*, 3297-3305.

39. Weigend, F. *Phys. Chem. Chem. Phys.* **2006***, 8*, 1057-1065.

40. Andrae, D.; Häußermann, U.; Dolg, M.; Stoll, H.; Preuß, H. *Theor. Chim. Acta* **1990***, 77*, 123-141.

41. Metz, B.; Stoll, H.; Dolg, M. *J. Chem. Phys.* **2000***, 113*, 2563-2569.

42. Grimme, S.; Antony, J.; Ehrlich, S.; Krieg, H. *J. Chem. Phys.* **2010***, 132*, 154104.

43. Grimme, S.; Ehrlich, S.; Goerigk, L. *J. Comput. Chem.* **2011***, 32*, 1456-1465.

44. Pipek, J.; Mezey, P. G. *J. Chem. Phys.* **1989***, 90*, 4916-4926.

45. NBO 6.0. Glendening, E. D.; Badenhoop, J. K; Reed, A. E.; Carpenter, J. E.; Bohmann, J. A.; Morales, C. M.; Landis, C. R., Weinhold, F. Theoretical Chemistry Institute, University of Wisconsin, Madison, **2013**.

46. Gaussian 09, Revision D.01, Frisch, M. J.; Trucks, G. W.; Schlegel, H. B.; Scuseria, G. E.; Robb, M. A.; Cheeseman, J. R.; Scalmani, G.; Barone, V.; Mennucci, B.; Petersson, G. A.; Nakatsuji, H.; Caricato, M.; Li, X.; Hratchian, H. P.; Izmaylov, A. F.; Bloino, J.; Zheng, G.; Sonnenberg, J. L.; Hada, M.; Ehara, M.; Toyota, K.; Fukuda, R.; Hasegawa, J.; Ishida, M.; Nakajima, T.; Honda, Y.; Kitao, O.; Nakai, H.; Vreven, T.; Montgomery, J. A., Jr.; Peralta, J. E.; Ogliaro, F.; Bearpark, M.; Heyd, J. J.; Brothers, E.; Kudin, K. N.; Staroverov, V. N.; Kobayashi, R.; Normand, J.; Raghavachari, K.; Rendell, A.; Burant, J. C.; Iyengar, S. S.; Tomasi, J.; Cossi, M.; Rega, N.; Millam, J. M.; Klene, M.; Knox, J. E.; Cross, J. B.; Bakken, V.; Adamo, C.; Jaramillo, J.; Gomperts, R.; Stratmann, R. E.; Yazyev, O.; Austin, A. J.; Cammi, R.; Pomelli, C.; Ochterski, J. W.; Martin, R. L.; Morokuma, K.; Zakrzewski, V. G.; Voth, G. A.; Salvador, P.; Dannenberg, J. J.; Dapprich, S.; Daniels, A. D.; Farkas, Ö.; Foresman, J. B.; Ortiz, J. V.; Cioslowski, J.; Fox, D. J. Gaussian, Inc., Wallingford CT, **2013**.

Table of Contents entry

A five-membered $PdSb_n$ coordination series

Andrew Jolleys, Benjamin R. M. Lake, Tobias Krämer* and Sophie L. Benjamin*